NETWORKS AND HETEROGENEOUS MEDIA
©American Institute of Mathematical Sciences
Volume **5**, Number **3**, September **2010**
doi:10.3934/nhm.2010.5.xx
pp. **1–xx**

APPLICATION OF A COUPLED FV/FE MULTISCALE METHOD TO CEMENT MEDIA

Thomas Abballe

CEA Saclay
DEN/DM2S/SFME/LSET Bat 454
91191 Gif-sur-Yvette Cedex , France

Grégoire Allaire

Conseiller Scientifique du DM2S – CEA Saclay
Centre de Mathématiques Appliquées – École Polytechnique
91128 Palaiseau Cedex, France

Éli Laucoin and Philippe Montarnal

CEA Saclay
DEN/DM2S/SFME/LSET Bat 454
91191 Gif-sur-Yvette Cedex , France

Abstract. We present here some results provided by a multiscale resolution method using both Finite Volumes and Finite Elements. This method is aimed at solving very large diffusion problems with highly oscillating coefficients. As an illustrative example, we simulate models of cement media, where very strong variations of diffusivity occur. As a by-product of our simulations, we compute the effective diffusivities of these media.After a short introduction, we present a theorical description of our method. Numerical experiments on a two dimensional cement paste are presented subsequently. The third section describes the implementation of our method in the calculus code *MPCube* and its application to a sample of mortar. Finally, we discuss strengths and weaknesses of our method, and present our future works on this topic.

1. Introduction.

1.1. Heterogeneities in cement media.

Cement media are spatially very heterogeneous with a large variety of physical scales. Furthermore the diffusivity of the cement components varies with a very large contrast of several orders of magnitude.

For example, when working on the *concrete* scale, where the representative elementary volume (REV) is roughly a few centimeters wide, we consider that the cement paste is homogeneous and that aggregates (sand, gravel) are scattered in it, thus creating millimiters wide heterogeneities.

On the other hand, if we choose to work at the *cement paste* scale (REV width not exceeding 100μm), we have to take into account mineral microstructures, which sizes range from 1 to 30μm. This is therefore a multiscale problem.

2000 *Mathematics Subject Classification.* 74Q05, 65N30.

Key words and phrases. finite volume method, finite element method, multiscale method, cement media.

This work was done in relation with the GNR MOMAS (Modélisation Mathématique et Simulations numériques liées aux problèmes de gestion des déchets nucléaires) (PACEN/CNRS, ANDRA, BRGM, CEA, EDF, IRSN).

1.2. **Determination of the effective diffusivity.** Our goal is to compute the effective diffusivity at the concrete or cement paste scale. This topic has previously been addressed by various laboratories at the CEA, the French Atomic Energy Commission, both from physical and mathematical points of view. Strict analytical homogeneization [6] can be, in this case, very complex to use, chiefly because of the continuous variation and the random spatial distribution of the inclusions (depending of the scale: aggregates or mineral stages).

A direct numerical simulation in three dimensions is almost impossible because of the huge computational resources (memory, CPU time) required by fine meshes. Therefore, in order to achieve our goal, we have developed a specific multiscale resolution method using both Finite Volumes (FV) and Finite Elements (FE) and we present here its preliminary results.

Many multiscale numerical methods have recently been developed and it is almost impossible to quote all the relevant works, be it Finite Elements methods [12], [14], [18], [20], [22] or Finite Volumes methods [17], [19].

1.3. **A FV/FE Multiscale method.** Our method relies on the coupling of two grids: a coarse one and a fine one. The main idea is to build a Finite Element basis on the coarse grid from solutions computed on the fine one. In previous works on this subject [5],[18], the Finite Element method was used on both the fine and coarse grids, whereas, in our approach, the fine scale simulations are made using Finite Volumes. Thus we expect to increase the stability of the method in view of strong discontinuities and anisotropy of the studied media, and to keep the advantages of the multiscale Finite Element method (no geometric assumptions on the media, easy parallelization of the computation).

We solve a stationary diffusion equation to determine the concentration C of a single chemical species:

$$\left\{ \begin{array}{rcll} -\nabla \cdot (D\,\nabla C) & = & \alpha & \text{in } \Omega, \\ C & = & f & \text{on } \Gamma_D, \\ D\,\nabla C \cdot n & = & g & \text{on } \Gamma_N, \end{array} \right. \tag{1}$$

where (Γ_D, Γ_N) is a partition of the boundary Γ of Ω.

2. **Description of the multiscale method.** In the sequel, Ω is either a rectangular domain (two dimensions) or a parallelepipedic one (three dimensions).

Algorithm 1 presents the various steps of our multiscale method we use for solving problem (1).

Algorithm 1 Main steps

1: Partition the domain into sub-domains with oversampling
2: Solve cell problems
3: Build the Finite Element basis
4: Solve the coarse problem
5: Compute the fine-scale solution

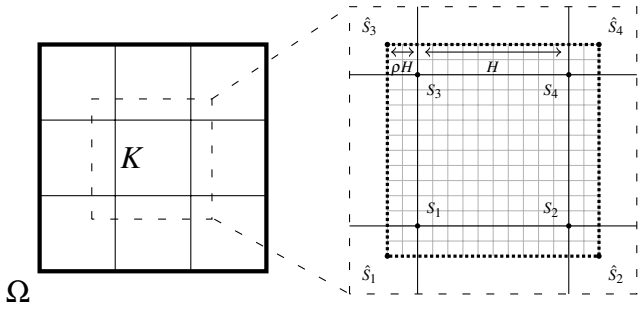

FIGURE 1. The domain Ω (bold line) is divided into rectangular macroelements K (solid line). The cell $\hat{K}$ (dotted line), built from K and a fraction ρ of its neighbours, is meshed finely (in thin grey).

2.1. **Decomposition into sub-domains with oversampling.** Assuming we know the diffusivity D on the fine scale, we divide the domain Ω into rectangular, respectively parallelepiped, macroelements K, thus creating a two-dimensional, respectively three-dimensional, regular coarse mesh. As shown in Figure 1, at the local scale, we define the cell $\hat{K}$ by enlarging the macroelement K with a fraction $\rho \geq 0$ of its neighbours. We call ρ the *oversampling rate*. Oversampling was introduced in [18] to improve the efficiency of multiscale finite element methods.

In order to save computing resources, the domain Ω is not globally meshed at the fine scale. The cells $\hat{K}$ are meshed individually, while ensuring that the meshes of two adjacent cells $\hat{K}_1$ and $\hat{K}_2$ are conforming on $\partial K_1 \cap \partial K_2$. Building smaller meshes for all cells than a large global mesh for the entire domain is of course much easier and efficient in terms of memory and CPU requirements. The fine scale meshes of $\hat{K}$ can be either structured or not.

2.2. **Solving cell problems.** With $n = 4$ (dimension 2) or $n = 8$ (dimension 3), let $(S_i)_{1\leq i\leq n}$ be the *vertices* of the macroelement K, and $(\hat{S}_i)_{1\leq i\leq n}$ the *vertices* of the cell $\hat{K}$.

On each cell $\hat{K}$ we have to solve a *cell problem* for each $1 \leq i \leq n$:

$$\left\{ \begin{array}{rl} -\nabla \cdot (D\, \nabla \Psi^i_{\hat{K}}) = 0 & \text{in } \hat{K}\,, \\ \Psi^i_{\hat{K}} = \beta^i & \text{on } \partial\hat{K}, \end{array} \right. \tag{2}$$

where β^i is a continuous linear function on each edge of $\partial\hat{K}$, with $\beta^i(\hat{S}_j) = \delta_{i,j}$, where δ stands for the Kronecker symbol.

For two-dimensional structured meshes it is possible to solve the cell problems by the *VF9 finite volume* method [16]. In most cases, as D is diagonal, this method is equivalent to the classical five points Finite Volume method. However, for more general cases we switched to the Diamond Finite Volume Method (*VFDiam*) for solving *cell problems*. First described in [11], *VFDiam* has been used by the CEA to work on media, like the cement ones, where strong anisotropies or/and contrasts of diffusivity occur. We now briefly recall the principles of *VFDiam*.

As shown in Figure 2 (left part), in the $2D$ case, we consider two adjacent cells where the unknowns, C^- and C^+ respectively, are located at their barycenter, and call $F = T_0T_1$ their common edge. We suppose D to be constant on each cell, equal to D^- and D^+ respectively.

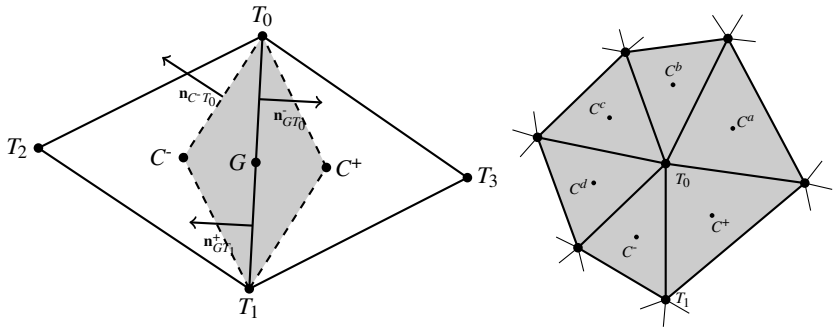

FIGURE 2. Left: a *VFDiam* element (in grey surrounded by a dashed line) is defined around the common face of two adjacent elements. Right: the set $\mathbb{T}_0$ (in grey) is defined as the collection of all cells which contain the node T_0.

We define the *VFDiam* volume as the union of the two half-diamond cells $T_0T_1C^-$ and $T_0T_1C^+$, respectively of volumes V^- and V^+. We then introduce G, the barycenter of F, and the intermediate unknowns C_{T_i} localised on T_i.

As a Finite Volume Method, the *VFDiam* method relies on the following approximation of the flux across F :

$$\int_F D\nabla C.\mathbf{n} = \frac{\mathbf{n}.\kappa^-\mathbf{n}\mathbf{n}.\kappa^+\mathbf{n}}{\mathbf{n}.\kappa^-\mathbf{n}+\mathbf{n}.\kappa^+\mathbf{n}}(C^+ - C^-) + \sum_{k=0}^{1}\left[\frac{\mathbf{n}.\kappa^+\mathbf{r}^+_{\mathbf{k}}\mathbf{n}.\kappa^-\mathbf{n}+\mathbf{n}.\kappa^-\mathbf{r}^-_{\mathbf{k}}\mathbf{n}.\kappa^+\mathbf{n}}{\mathbf{n}.\kappa^-\mathbf{n}+\mathbf{n}.\kappa^+\mathbf{n}}\right]C_{T_k} \tag{3}$$

where:

- $\mathbf{n}$ is the normal vector of F, oriented from C^- to C^+ and of norm $\|F\|$.
- $\kappa^- = \frac{D^-}{2V^-}$, respectively $\kappa^+ = \frac{D^+}{2V^+}$
- $\mathbf{r}^-_{\mathbf{k}} = \mathbf{n}_{C^-T_k} + \mathbf{n}^-_{GT_k}$ et $\mathbf{r}^+_{\mathbf{k}} = \mathbf{n}_{C^+T_k} + \mathbf{n}^+_{GT_k}$
- $\mathbf{n}^-_{GT_k}$ is the normal vector of $[GT_k]$, oriented outward $T_0T_1C^-$, of norm $\|GT_k\|$

As we have introduced the intermediate unknown C_{T_i}, we need an additionnal relation to keep the problem well-posed. It is provided by a least squares interpolation method on $\mathbb{T}_i$, the set of cells incident to the node T_i (cf. Figure 2, right part). For all nodes, C_{T_i} is computed as a linear combination of the unknowns C_j associated with cells in $\mathbb{T}_i$.

A similar formula exists for the three-dimensional case. It can be found in [2], as well as the detailed calculation of (3).

2.3. **Definition of the finite element basis.** On each macroelement K, we construct $(\Phi^i_K)_{1\le i\le n}$ by linear combination of the functions $(\hat{\Psi}^i_{\hat{K}})_{1\le i\le n}$, solutions of (2). To find the coefficients $a_{i,l}$, we impose, for any $1 \le i \le n$, that

$$\forall\, 1 \le j \le n \quad \Phi^i_K(S_j) = \sum_{1\le l\le n} a_{i,l}\Psi^l_{\hat{K}}(S_j) = \delta_{i,j}.$$

Let $\mathcal{I}$ be the set of nodes of the coarse grid, and $N_{\mathcal{I}}$ the cardinal of $\mathcal{I}$. The finite element function Φ^I, associated to $I \in \mathcal{I}$, is defined piecewise on each macroelement $K \ni I$. Provided I coincides with a vertex of K, i.e. $S_j = I$, we have:

$$\Phi^I_{|K} = \Phi^j_K.$$

Due to the oversampling of cells $\hat{K}$, the *Finite Element* basis $(\Phi^I)_{I\in\mathcal{I}}$ is non-conforming, namely each Φ^I is discontinuous through the boundary ∂K of the macroelement K.

A strict oversampling of macroelements is not mandatory to properly define the multiscale method. We can choose $\rho = 0$ and then have $\hat{K} = K$. In such a case, this step of the method becomes trivial as we have $\Phi^i_K = \Psi^i_{\hat{K}}$. However, when $\rho = 0$, the multiscale method is less efficient because of a *boundary layer resonance*, due to the use of linear boundary conditions to solve the cell problems (§2.2). Quantitative and qualitative effects of the oversampling rate ρ are detailed in [14].

2.4. **Solving the coarse problem.** We solve the coarse problem by a *Finite Element Method* relying on the basis $(\Phi^I)_{I\in\mathcal{I}}$. It amounts to solve the linear system

$$\mathbb{K}\mathbf{C}_H = \mathbf{S},$$

with $\mathbb{K}$ a square matrix of size $N_{\mathcal{I}}$, defined by

$$\mathbb{K}(I,J) = \int_\Omega D\nabla\Phi^I \cdot \nabla\Phi^J \quad \forall (I,J) \in \mathcal{I},$$

and $\mathbf{S}$ a column vector deduced from the data f, g and α in (1) with matrices similar to $\mathbb{K}$. We build those matrices by assembling their local counterparts, which allows us to distribute calculus on various processors:

$$\mathbb{K}_K(i,j) = \int_K D\nabla\Phi^i_K \cdot \nabla\Phi^j_K \quad \forall\, 1 \le i,j \le n.$$

We compute these terms, at the fine scale, from the *VFDiam* approximation of fluxes (3), applied to $(\Phi^i_K)_{1\le i\le n}$.

2.5. **Computing the fine-scale solution.** Last but not least, we reconstruct, at the fine scale, the solution C, by weighting the function $(\Phi^I)_{I\in\mathcal{I}}$ with the values of the coarse solution

$$C = \sum_{I\in\mathcal{I}} \mathbf{C}_H(I)\Phi^I \ .$$

As the pratical interest of this method is to solve *very large problems*, where a classical resolution is technically impossible, we usually can not store the reconstructed solution C (or its gradient or its flux density $\|D\nabla C\|$) on the whole domain in a single array. Rather, we reconstruct the solution on subdomains of interest, thus handling arrays of smaller size, fitting in the available computer memory.

This is achieved by gluing solutions of adjacent macroelements, and this is the reason why we need to ensure that meshes are conforming across the boundaries of macroelements (cf. §2.1). However, as the Finite Element method is not conforming, this does not impose any kind of continuity on the solution.

2.6. **Estimate of the computational cost.** We assume that the domain Ω is divided into M macroelements and that each macroelement K is meshed with N microscopic elements. Taking into account the oversampling area, each cell $\hat{K}$ contains about $(1+2\rho)^d N$ elements, with d the space dimension. We note $\mathcal{F}(\mathcal{N})$ a function estimating the cost of solving a linear problem of size $\mathcal{N}$.

The total cost, in computational time, of our multiscale method can be estimated by:

$$\mathcal{C}^{tot} = \underbrace{M \times \mathcal{F}((1+2\rho)^d N)}_{\text{Solving cell problems}} + \underbrace{\mathcal{F}(M)}_{\text{Coarse problem}} + M \times O(N), \tag{4}$$

where we use the Landau notation $O(N)$ for a function of order N at infinity. It is only an approximation of the computational cost of our method, as the costs of some minor operations have been neglected. The rightmost term of (4) represents the cost of assembling Finite Element matrices (§2.4) and of reconstructing the fine-scale solution from the coarse one (§2.5).

Estimate (4) can be compared, for example, to a direct resolution by the Finite Element or Finite Volume method, the cost of which would be $\mathcal{F}(MN)$. Considering that usually $\mathcal{F}(MN) = O(M^3N^3)$ for a direct solver on a full matrix, or $\mathcal{F}(MN) = O(M^2N^2)$ for an iterative solver on a sparse matrix, we can see that the multiscale method is far less expensive than the direct ones. Of course, this low computational cost has a counterpart: results obtained by the multiscale method are, by principle, less accurate.

We would like to emphasize that every step of the multiscale method can be done in parallel but one: solving the coarse problem (§2.4). Therefore, provided we have enough processors, of the order of M, we can expect a very low computational cost on parallel computers:

$$\mathcal{C}^{tot} = \mathcal{F}((1+2\rho)^d N) + \mathcal{F}(M) + O(N). \tag{5}$$

3. Application to a cement paste model.

3.1. **Description of the cement paste.** We consider a cement paste as described by previous CEA works [7]. In this section, lengths are expressed in *micrometers* (μm). The square domain $\Omega = [0,100]^2$ is composed of a porous phase, of diffusivity $D_0 = 2.2 \times 10^{-9} \mathrm{m}^2 \cdot \mathrm{s}^{-1}$, filled with thousands of inclusions representing the various minerals existing in concrete. Depending on their caracteristics (average size, number of layers and diffusivity), inclusions are dispatched into four groups:

- 3500 homogeneous spheres (diffusivity $d_1 = 1 \times 10^{-20} \mathrm{m}^2 \cdot \mathrm{s}^{-1}$, radius $r_1 \in [0.1, 1.3]$) for the portlandite, aluminates and anhydrides.
- 1700 homogeneous spheres (diffusivity $d_2 = 1 \times 10^{-12} \mathrm{m}^2 \cdot \mathrm{s}^{-1}$, radius $r_2 \in [0.1, 1.3]$) of HD C-S-H (*High Density* C-S-H).
- 1900 homogeneous spheres (diffusivity $d_3 = 9 \times 10^{-12} \mathrm{m}^2 \cdot \mathrm{s}^{-1}$, radius $r_3 \in [0.1, 1.3]$) of LD C-S-H (*Low Density* C-S-H).
- 200 multi-layer spheres (radius $r_4 \in [1.3, 2.8]$) composed of a core of portlandite (stretching on the first 40% of the radius) and two shells: one of HD C-S-H (from $0.4r_4$ to $0.9r_4$) and one of LD C-S-H (from $0.9r_4$).

The random spatial distribution of the inclusions is computed by a program developped by Erwan Adam [3]. Figure 3 presents a close-up of the domain.

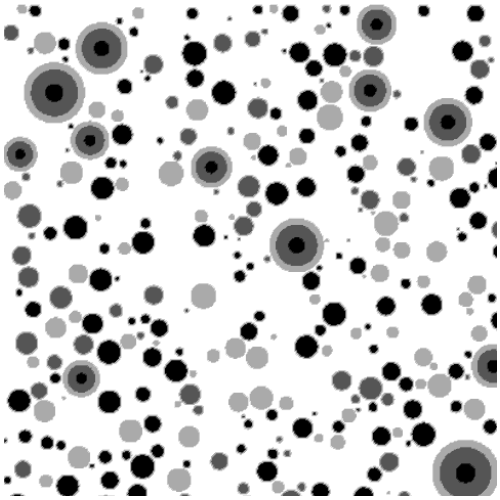

FIGURE 3. Close-up of the cement media: pore phase (white), LD C-S-H (light grey), HD C-S-H (dark grey), portlandite, aluminates and anhydrides (black).

3.2. **Two-dimensional simulation .** We present here our first numerical experiments. They used the *VF9* Finite Volume method, and both the coarse and fine scale meshes are rectangular and structured.

We solved the following problem:

$$\left\{\begin{array}{rcll} -\nabla\cdot(D\,\nabla C) & = & 0 & \text{on } \Omega=[0,100]^2,\\ C(0,y) & = & 1 & \text{for } y\in[0,100],\\ C(1,y) & = & 0 & \text{for } y\in[0,100],\\ D\,\nabla C\cdot n & = & 0 & \text{if } y\in\{0,100\}. \end{array}\right. \tag{6}$$

With these specific conditions, we can compute a physical value of the *homogenized coefficient* from the ingoing and outgoing fluxes, themselves computed from the fine scale solution:

$$D^\star = \frac{1}{L}\int_{\{x=100\}} D\nabla C\cdot n, \tag{7}$$

where $L=100$ is the length of the domain. We emphasize that the homogenized coefficient computed by (7) is *not* the theorical homogenized coefficient as defined by *homogenization theory* [4]. This formula for $D^\star$ has been chosen in order to mimic the experimental measurements of equivalent diffusivity.

The homogenized coefficient $D^\star$ computed by our method is displayed on Figure 4. The number of macroelements K is fixed to 100 as we increase the number of fine scale elements. The coefficient follows a similar evolution for the four values of ρ we tried, matching the figures computed from the direct resolution (solid line) from less that 10%. However, we can not really consider that our homogenized coefficient converges.

This gap is linked to the flux density error, presented on Figure 5. We note that the error is up to 5 times stronger near the boundaries of macroelements K. This *boundary layer resonance*, described in [14], is usually limited by the oversampling method. However this is not the case here. At best, for $\rho=0.05$, we decrease the

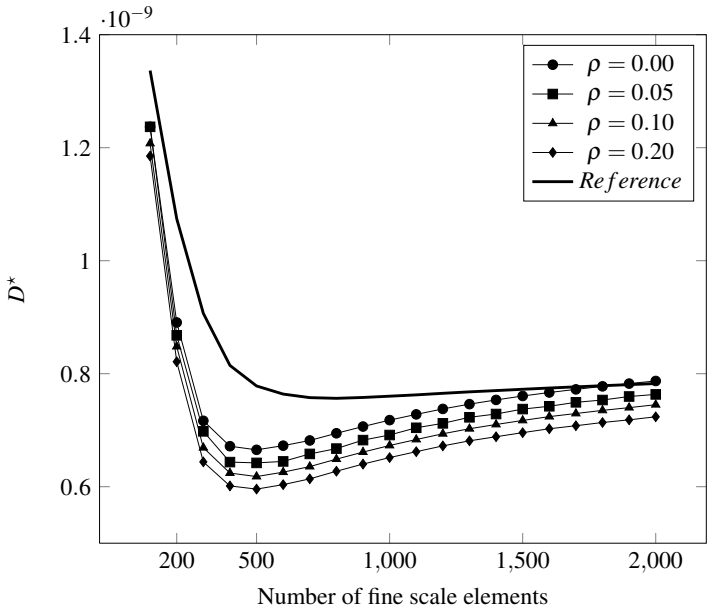

FIGURE 4. Evolution of the homogenized coefficient, with a fixed number M of macroelements, when the precision of the fine-scale mesh increases. The reference solution is computed from a direct resolution of problem (1).

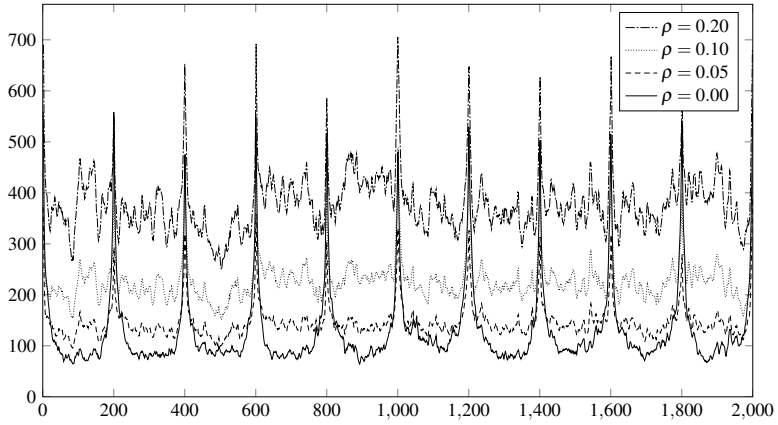

FIGURE 5. Cut across the domain Ω of the flux density: difference between the multiscale method ($M = 10 \times 10$) and the reference solution.

maximal error values by 30%, but we also *increase* the minimal error value. In the end, the mean error value increases.

4. **Application to a sample of mortar .**

4.1. **A $3D$ implementation in a parallel environment.**

As shown in section §3, the results computed with our first implementation highlighted some weaknesses

[1]. To improve the method, an important work of implementation has been made, and is presented in this section. Indeed, to increase its performances, the method has been integrated into the parallel numerical code *MPCube* [9], itself relying upon the calculus kernel *Trio-U* [23].

It allows us to easily solve 2D and 3D diffusion problems by the *VFDiam* method, both in sequential and parallel contexts. Our method can now use two levels of parallelism. The *outer-cell* parallelism (see §2.6) allows us to process the work on each cell independently from each other. The *inner-cell* parallelism, using a parallel solver for the computations on each cell, increases our computational capacities to manipulate and solve even larger problems. Applied to the expensive steps of the method, namely meshing the cells and solving the cell problems, these two levels of parallelism broaden significantly our choice of parameters for the multiscale method. For example, we are now able to mesh very accurately each oversampling area and, by extension, to choose the oversampling rate ρ with more precision.

4.2. **Description of the mortar.** We want to conduct simulations on a sample of mortar. In mortars, grains of sand are not directly contiguous to the paste, they are wrapped with highly diffusive *transition layers*. These layers play a prominent part in the transport of chemical species. Indeed, whereas grains of sand are necessarly distinct, the various transition layers can merge with each other. When the density of sand increases, highly diffusive pathes appear through the media, a phenomenon called *percolation* [8].

Experimental processes have estimated the thickness of the transition layers to 30μm, whereas the diameter of grains of sand stretches from 0.16 to 4mm. In order to deal with this wide range in the characteristic lengths, we usually need to work with very fine discretizations, which leads to huge meshes. This is exactly a case where a multiscale method is useful: we can mesh very accurately each part of the domain, with their sand grains and the corresponding layers, but as the domain has been subdivided, each mesh remains of acceptable size.

We consider here a 125mm^3 cubic domain. Like the cement media described in §3, it is modelised as a background media, of adimensionate diffusivity $D_b = 5$, filled with homogeneous spheres, the grains of sand, of diffusivity $D_s = 1$. Each sphere is then wrapped in a 30μm layer of diffusivity $D_t = 15$ acting as a transition zone. We suppose that the transition zones remain distinct from each other, even if it is physically unlikely as we chose the sand volume fraction to be quite high (35%). Diffusivity values come from measures by mercury intrusion porosimetry [8], while the size distribution of sand grains, shown in Figure 6, comes from industrial granulometric measurements [13].

4.3. **Numerical experiments.** The domain is meshed by 125 cubic macroelements (5 in each space direction) with no oversampling ($\rho = 0$). Each cell is then meshed by the tools $GHS3D$ and $BLSURF$ via the $SALOME$ platform [21]. The number of mesh elements in each cell varies from 1×10^5 to 5×10^5, depending on the local geometry of the cell. For example, tangent points between spherical inclusions and the cell boundaries lead to an important increase of the number of tetrahedrons needed to mesh the cell appropriately. This adds up to approximately 2×10^7 elements in the whole domain. Figure 7 presents the mesh for one cell, composed of approximatively 2.5×10^5 elements.

We solve problems which are $3D$ transcriptions of problem (6) used in §3.2. We impose as boundary conditions $C = 1$ when $x = 0$, $C = 0$ when $x = 5$ and a null

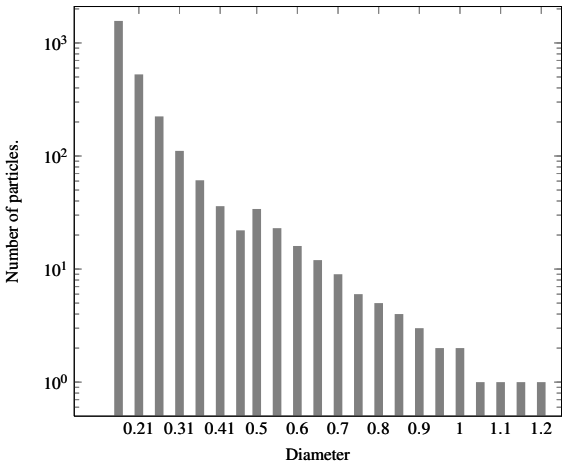

FIGURE 6. Size distribution of sand grains in the mortar, computed from the sand granulometric curves. The biggest sizes of sand grains, from 1.2mm to 4mm, are here dismissed, as the domain is only 5mm wide.

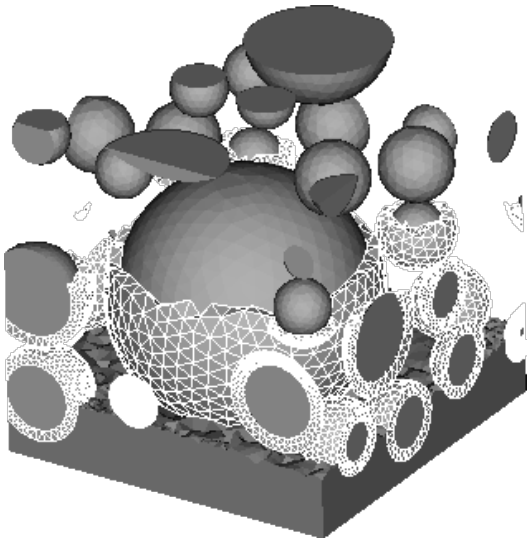

FIGURE 7. Geometry and mesh of one cell. Cement paste (bottom) has been clipped in order to show the spherical sand grains and the matching transition layers (highlighted, clipped on the top).

flux on the other sides. Finally, we choose a null source term. Figure 8 displays the evolution of the concentration C with x, whereas the other coordinates $(y; z)$ are constant. Both global and local phenomena are observed. From a global point of view, the solution C appears almost linear. However, strong variations can occur on very short distances when the chemical species crosses a highly diffusive transition layer.

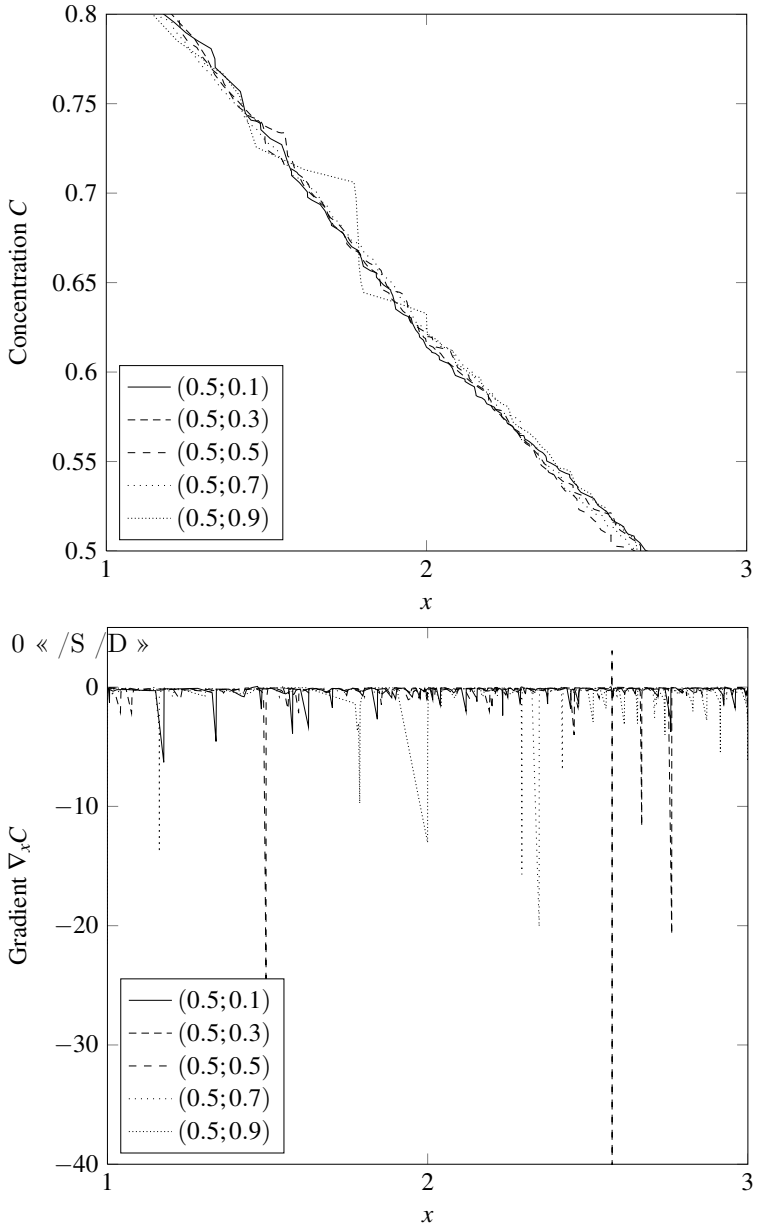

FIGURE 8. Concentration C and longitudinal gradient $\nabla_x C$ across the domain, from $x = 1$ to 3, whereas the remaining coordinates $(y; z)$ are constant. The transition layers are easily recognized by the small jumps they induce in the concentration profiles.

In a future analysis of those results, we will compute the *homogenized coefficient* $D_x^\star$ from the ingoing and outgoing fluxes using (7). By switching the boundary conditions from face to face, we will compute 3 homogenized coefficients $D_x^\star$, $D_y^\star$

and $D_z^\star$. We work here on a representative element of the mortar, which is expected to be isotropic. Consequently, the coefficients should be roughly the same.

5. **Conclusions and future works.** We have presented some numerical experiments using our coupled FV/FE multiscale method. They were first computed with our standalone $2D$ implementation, then with the parallel numerical code *MPCube*.

In the 2D case, our method has shown promising results, but also some weaknesses [1]. Actually, the method converges smoothly for academic benchmarks, but the error tends to stall in the cement media cases because of a boundary layer effect. Our first attempt to solve this problem, by oversampling the coarse elements, has not been successful yet because of the large contrast of diffusivity. To circumvent this difficulty we have emphasized two directions of work.

We have first focused on the oversampling method. It requires a very accurate mesh on each oversampling area and a well-chosen oversampling rate ρ [14]. Using such precision would exceed the computational capacities of our first implementation. Consequently our method was integrated into the parallel numerical code *MPCube*. This new implementation has been tested on a realistic $3D$ case of mortar. More numerical experiments will be conducted, especially comparisons with large size direct resolutions as part of the EHPOC project [15].

Second, it has been made clear that the non-conformity of the Finite Element basis at the coarse scale is the main obstacle for convergence when the oversampling rate ρ is not small. To overcome this problem we plan to use Discontinuous Galerkin methods [10] to solve the coarse problem, instead of a classical Finite Element method.

REFERENCES

[1] T. Abballe, "Une Méthode Multi-échelle Couplée Volumes et Éléments Finis. Application aux Matériaux Cimentaires," Internal CEA Report SFME/LSET/RT/08/003/A, CEA, DEN/DM2S, November 2008.

[2] S. Abide and F. Caro, *Maquette solveur volumes finis multi-physique*, Internal CEA Report SFME/MTMS/RT/07-005/B, CEA, DEN/DM2S, June 2007.

[3] E. Adam, P. Montarnal, B. Bary, H. Peycelon and C. Gallé, *Chaîne de calcul pour la dégradation sous eau des bétons: méthodologie, outil et illustration*, Internal CEA Report SFME/MTMS/RT/07-0006/A, CEA, DEN/DM2S, May 2007.

[4] G. Allaire, *Shape optimization by the homogenization method*, Applied Mathematical Sciences, vol. **146**, Springer, 2001.

[5] G. Allaire and R. Brizzi, *A multiscale finite element method for numerical homogenization*, Multiscale Modeling and Simulation, **4** (2005), 790–812.

[6] S. Bejaoui and B. Bary, *Modeling of the link between microstructure and effective diffusivity of cement pastes using a simplified homogenization method*, Cement and Concrete Research, **37** (2007), 469–480.

[7] S. Bejaoui, B. Bary and C. Julien, *Modélisation de la relation entre microstructure et diffusivité effective des pâtes de ciment à partir d'une méthode numérique 3d*, Internal CEA Report DPC/SCCME/05-327-A, CEA, Département de Physico-Chimie, January 2006.

[8] B. Bourdette, E. Ringot and J. P. Ollivier, *Modelling of the transition zone porosity*, Cement and concrete research, **25** (1995), 741–751.

[9] F. Caro and E. Laucoin, "Description du Module MPCube Permettant la Simulation Numérique des Écoulements Diphasiques à deux Composants en Milieu Poreux," Internal CEA Report SFME/LSET/RT/09-006/A, CEA, DEN/DM2S, April 2009.

[10] B. Cockburn, *Discontinuous galerkin methods*, ZAMM - Journal of Applied Mathematics and Mechanics, **83** (2003), 731–754.

[11] Y. Coudière, J-P. Vila and P. Villedieu, *Convergence rate of a finite volume scheme for a two dimensional convection-diffusion problem*, Mathematical Modelling and Numerical Analysis, **33** (1999), 493–516.

[12] W. E and B. Engquist, *The heterogeneous multiscale methods*, Communications in Mathematical Sciences, **1** (2003), 87–132.
[13] T. Eder, H. Rötzer, D. Donhoffer, L. Riedlmayer, W. Volkmann, K. Wallisch and J. Zöhrer, *Online measurement of the grain size distribution of sand 0-4 mm used for the production of concrete*, Particle and Particle Systems Characterization, **1** (1984), 85–88.
[14] Y. R. Efendief, T. Y. Hou and X-H. Wu, *Convergence of a nonconforming multiscale finite element method*, SIAM Journal of Numerical Analysis, **37** (2000), 888–910.
[15] *Environnement Haute Performance pour l'Optimisation et la Conception*, http://www.systematic-paris-region.org/fr/UserFiles/File/EHPOC.pdf.
[16] I. Faille, *A control volume method to solve an elliptic equation on a two-dimensional irregular mesh*, Comput. Methods Appl. Mech. Eng., **100** (1992), 275–290.
[17] H. Hajibeygi, G. Bonfigli, M. A. Hesse and P. Jenny, *Iterative multiscale finite-volume method*, Journal of Computational Physics, **227** (2008), 8604–8621.
[18] T. Y. Hou and X-H. Wu, *A multiscale finite element method for elliptic problems in composite materials and porous media*, Journal of computational physics, **134** (1997), 169–189.
[19] P. Jenny, S. H. Lee and H. A. Tchelepi, *Multiscale finite-volume method for elliptic problems in subsurface flow simulation*, Journal of Computational Physics, **187** (2003), 47–67.
[20] A. M. Matache, I. Babuška and C. Schwab, *Generalized* p-*FEM in homogenization*, Numerische Mathematik, **86** (2000), 319–375.
[21] *Plate-forme SALOME*, http://www.salome-platform.org/.
[22] C. Schwab and A. M. Matache, *Multiscale and multiresolution methods: Theory and applications*, Lecture Notes in Computational Science and Engineering, vol. **20**, ch. Generalized FEM for Homogenization Problems, 197–238, Springer Verlag, 2002.
[23] *Trio-U*, http://www-trio-u.cea.fr/.

Received January 2010; revised June 2010.

E-mail address: thomas.abballe@cea.fr
E-mail address: gregoire.allaire@polytechnique.edu
E-mail address: philippe.montarnal@cea.fr
E-mail address: eli.laucoin@cea.fr